

pubs.acs.org/cm Article

Family of Mo₄Ga₂₁-Based Superconductors

Valeriy Yu. Verchenko,* Alexander O. Zubtsovskii, Danil S. Plenkin, Alexey V. Bogach, Zheng Wei, Alexander A. Tsirlin, Evgeny V. Dikarev, and Andrei V. Shevelkov



Cite This: Chem. Mater. 2020, 32, 6730-6735



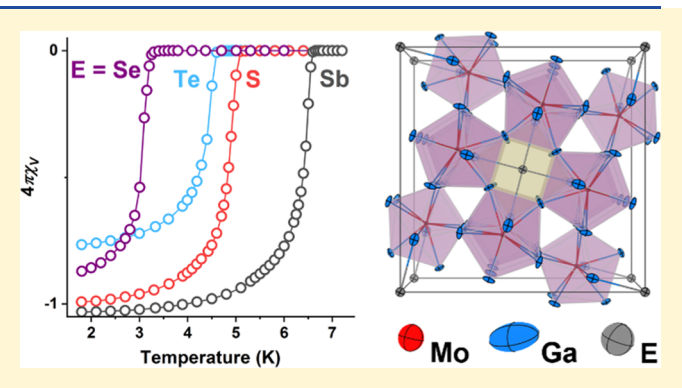
ACCESS

Metrics & More

Article Recommendations

SI Supporting Information

ABSTRACT: Endohedral cluster superconductors are an emerging field, where simple electron counting rules govern the phase stability and transition temperature. Nontrivial microscopic properties of the superconducting state, including strong electron—phonon coupling and multigap superconductivity, raise fundamental interest in studying these materials. Herein, $\text{Mo}_4\text{Ga}_{20,38(1)}\text{S}_{0.62(1)}$, $\text{Mo}_4\text{Ga}_{20}\text{Se}$, $\text{Mo}_4\text{Ga}_{20}\text{Te}$, and $\text{Mo}_4\text{Ga}_{20}\text{Sb}$ endohedral cluster compounds were synthesized in the form of bulk polycrystalline samples and single crystals. Together with the recently reported $\text{Mo}_4\text{Ga}_{21-x-\delta}\text{Sn}_{x}$, these compounds belong to the new $\text{Mo}_4\text{Ga}_{21}$ structure type with notable functionality: all the discovered representatives show superconducting properties. The observed critical temperatures of 5.1, 3.3, 4.6, and 6.6 K for the S-,



Se-, Te-, and Sb-containing compounds, respectively, correlate well with the experimental values of the Sommerfeld coefficient. An emerging role of the electron–phonon coupling may be responsible for the enhancement of critical temperature in the case of $Mo_4Ga_{20}Sb$.

ntermetallic compounds composed of metals from different blocks of the periodic table provide a rich source of functional materials. The functionality can be inherent in a family of compounds with a common structural motif. For example, IrIn₃- and Ir₃Ge₇-type compounds represent two structural families showing a large number of narrow-gap semiconductors¹⁻⁵ with promising thermoelectric properties.^{2,6} Interestingly, semiconducting properties appear at a particular number of valence electrons, 17 e for the IrIn₃-type compounds and 55 \overline{e} for the Ir₃Ge₇ structure type. Within the family of Nowotny chimney ladder compounds, semiconducting intermetallics are found with a valence electron count of VEC = 14.7 Herein, higher manganese silicides attract interest because of high thermoelectric performance.⁸ Functionality is even more pronounced in the family of Heusler compounds, which consists of binary, ternary, and quaternary intermetallics with the common cubic structural motif.9 In this family, narrow-gap semiconductors yield efficient thermoelectric materials. ^{10,11} In addition to normal semiconductors, there are zero-gap semiconducting Heusler compounds, in which strong spin-orbit coupling leads to band inversion in the electronic structure. For those zero-gap semiconductors, which contain rare earth metals, multifunctional behavior was reported including induced antiferromagnetism in GdPtBi and ErPtBi, 12 heavy-fermion behavior in YbPtBi, 13 and superconductivity in LaPtBi¹⁴ and YPtBi.¹⁵

Intermetallic families, such as IrIn₃-type phases, both Nowotny chimney ladders and Heusler compounds, exhibit

inherent functionality, which depends on the number of valence electrons. Semiconducting properties at the particular values of VEC are associated with the stable electronic configurations, such as an 8-electron configuration in the main group MgAgAs-type compounds¹⁶ and an 18-electron configuration in the transition-metal-based intermetallics.^{17–19} At the same time, superconductivity is usually found in the metallic state with the increased number of valence electrons, when the Fermi level is shifted to the conduction band and high density of states is realized at the Fermi energy. This scheme was proposed to describe the physical properties of the endohedral Ga cluster compounds, where a number of superconductors, including Mo₈Ga₄₁, ^{20,21} Mo₆Ga₃₁, ^{22,23} ReGa₅, ²⁴ Rh₂Ga₉, ²⁵ and Ir₂Ga₉, ²⁵ exhibit a peculiar dependence of the critical temperature on the valence electron count.

Recently, we reported on the new endohedral cluster superconductor $Mo_4Ga_{21-x-\delta}Sn_x$ with $T_c=5.85$ K. Here, we further extend the Mo_4Ga_{21} structure type by synthesizing the $Mo_4Ga_{20.38(1)}S_{0.62(1)}$, $Mo_4Ga_{20}Se$, $Mo_4Ga_{20}Te$, and $Mo_4Ga_{20}Se$ compounds and explore their physical properties. Our study reveals that superconductivity is inherently present

Received: June 3, 2020 Revised: July 8, 2020 Published: July 9, 2020





in the Mo₄Ga₂₁-based compounds giving rise to a new intermetallic family of superconducting materials.

The Mo₄Ga₂₁-based compounds, namely, $Mo_4Ga_{20.38(1)}S_{0.62(1)}$ (1), $Mo_4Ga_{20}Se^{-}(2)$, $Mo_4Ga_{20}Te^{-}(3)$, and Mo₄Ga₂₀Sb (4), can be synthesized in the form of bulk polycrystalline samples or submillimeter-size single crystals (see Supporting Information for more details). In the first case, annealing of the elements taken in the Mo₄Ga_{21-x}E_x proportions is used, where E = S, Se, Te, Sb. (2), (3), and (4) can be synthesized exactly from the stoichiometric mixtures, while in the case of E = S, the x = 0.5 and x =0.75 starting compositions yield phase-pure samples (see Table S1 of Supporting Information). The crystal growth can be performed using the joint flux technique.²⁸ For example, the $Mo(Ga_{1-\nu}Te_{\nu})_{50}$ sample with the joint excess of Ga and Te can be annealed at a high temperature of 1000 °C and slowly cooled down, yielding large bulky crystals of GaTe and small needle-like single crystals of (3) for y = 0.05.

The crystal structure of (3), which is representative for the title Mo₄Ga₂₁-based compounds, is shown in Figure 1 (see

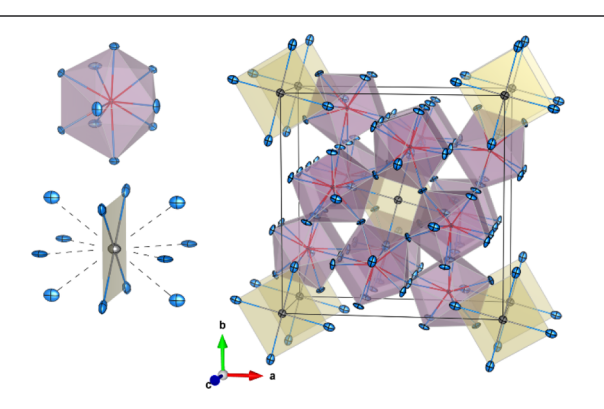


Figure 1. Crystal structure of $Mo_4Ga_{20}Te$ showing the unit cell and principal polyhedra. Mo atoms are drawn in red, Ga in blue, and Te in grey.

Supporting Information, Tables S2-S10 for complete structural information). In the structure adopting the I4/mspace group, Mo atoms are embedded inside the peculiar Mo@Ga₁₀ clusters, which can be viewed as a junction of a one half of a cube with one half of an icosahedron. The Mo@Ga₁₀ clusters share their triangular faces with the Te@Ga12 cuboctahedron centered at the (0; 0; 0) position, such that eight Mo@Ga₁₀ clusters surround one Te@Ga₁₂ cuboctahedron. The cuboctahedron is significantly distorted such that Te atoms have four short (2.9 Å) and eight long (3.3 Å) contacts with Ga atoms (full list of interatomic distances is given in Supporting Information, Table S7). Thus, the actual coordination polyhedron of Te can be viewed as a square of Ga atoms. In the case of (1), (2), and (3), the (0; 0; 0) position may contain statistically mixed Ga and chalcogens, when the composition deviates from the stoichiometric one; moreover, in the case of (1) only off-stoichiometric compositions can be synthesized in agreement with the previous report.²⁷ On the contrary, (4) demonstrates a much narrower compositional range. In fact, only the stoichiometric composition of Mo₄Ga₂₀Sb with the (0; 0; 0) position fully occupied by the Sb atoms can be isolated.

In the (1)–(4) series, the a parameter of the tetragonal unit cell elongates with the increase of the atomic number of E, but the c parameter does not show such monotonic behavior (see

Supporting Information, Table S2). For the Mo_4Ga_{21} -based compounds, the molar volume can be calculated using volume increments of the constituents. This simple approach apparently results in the significant overestimation of the molar volume. However, the experimental values of V demonstrate linear behavior *versus* $V_{\rm calc}$ (Figure 2) indicating that the unit

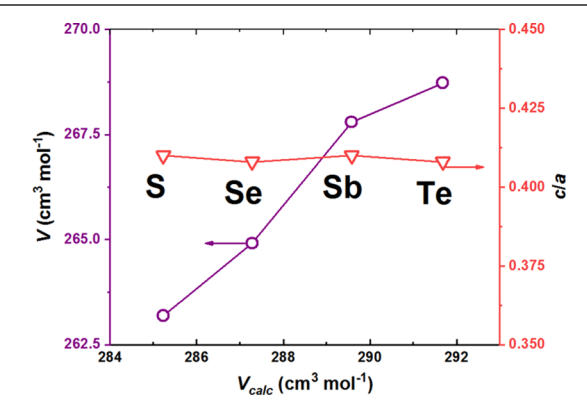


Figure 2. (Left axis) Experimental vs calculated molar volume and (right axis) the c/a unit cell parameter ratio for the Mo₄Ga₂₁-based compounds.

cell volume grows monotonously with the increase of E element atomic size. Moreover, the c/a ratio remains constant across the studied series, and the recently discovered isomorphous $Mo_4Ga_{21-x-\delta}Sn_x$ compound shows a similar value of c/a=0.42. Thus, five representatives of the Mo_4Ga_{21} -based family, including the E = S, Se, Te, Sb, and Sn compounds, compose the new intermetallic structure type. This structure type can be further combined with those of Mo_6Ga_{31} and Mo_8Ga_{41} , establishing a rich family of Mo-based endohedral cluster compounds because all the structures are built upon the same $Mo@Ga_{10}$ clusters.

The Mo₄Ga₂₁-based compounds possess similar electronic structures (see Supporting Information for more details). The valence orbitals of the E element (E = S, Se, Te, Sb) contribute to the electronic states on top of the valence band, where flat atomic-like electronic bands appear below relative energies of -1.5 eV for (1)–(3) and below -1 eV for (4). The electronic structures of the Mo₄Ga₂₁-based compounds depend significantly on the nature of the E element. When going from (1) and (2) to (3), and then to (4), electronic states on top of the valence band become flatter and form the peak substructure (see Supporting Information, Figure S2). The valence and conduction bands are separated by the dip of the density of states, and the Fermi level is situated in the conduction band ensuring the metallic behavior (Figure 3). The bottom of the conduction band is formed by the 4d states of Mo and 4p states of Ga atoms. Thus, the electronic properties of the Mo₄Ga₂₁-based compounds originate primarily from the mixing of Mo and Ga states with only negligible contribution from the E element. In each case, the high density of states at the Fermi energy is realized yielding the calculated Sommerfeld coefficient, γ_{bare} , larger than 15 mJ mol⁻¹ K⁻².

Measurements of electrical resistivity confirm metallic behavior of the Mo₄Ga₂₁-based compounds at temperatures above 10 K (detailed description of physical properties, including magnetic susceptibility, magnetization, electrical resistivity, and heat capacity, is given in the Supporting Information). In the same temperature range, small and

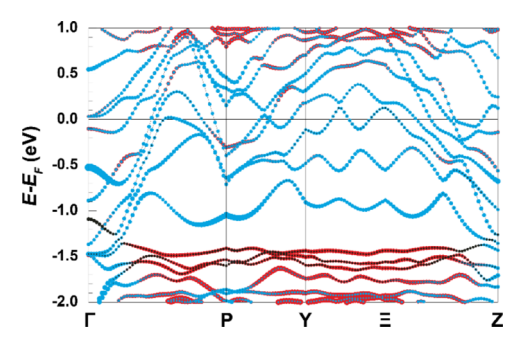


Figure 3. Electronic structure of $Mo_4Ga_{20}Te$ in the vicinity of the Fermi energy. Contribution of the Mo 4d states is shown in red, Ga 4p in blue, and Te 5p in black.

negative values of magnetic susceptibility indicate weak diamagnetic behavior. At low temperatures, the Mo_4Ga_{21} -based compounds demonstrate superconducting properties with the critical temperatures of $T_c = 5.1$ K, 3.3 K, 4.6 K, and 6.6 K in a zero magnetic field for (1)-(4), respectively (Figure 4). The bulk type-II superconductivity is confirmed by

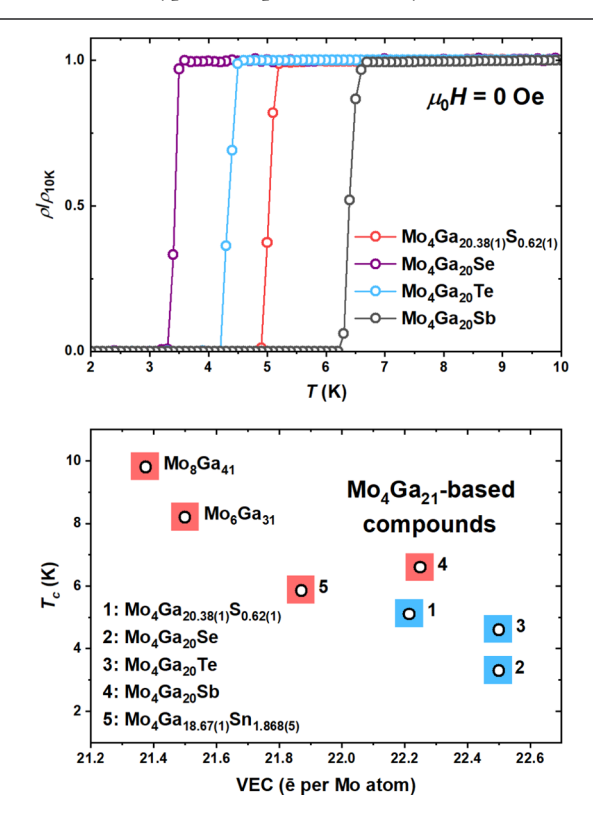


Figure 4. (Top) Low-temperature resistivity of the Mo_4Ga_{21} -based compounds in the zero magnetic field. (Bottom) Critical temperature of the Mo-based endohedral cluster superconductors as a function of valence electron count. Blue squares mark the superconductors with $\alpha = \alpha_{BCS}$ and red squares—the strong coupling superconductors with $\alpha > \alpha_{BCS}$.

resistivity, magnetization, and heat capacity measurements. Heat capacity measured in the superconducting and normal states was used to calculate the electronic contribution as $\Delta C_e/T = C/T(\mu_0 H = 0 \text{ T}) - C/T(\mu_0 H = 3 \text{ T})$, which was analyzed within the Bardeen–Cooper–Schrieffer (BCS) theory and the derived α -model. In the case of (1)–(3), the electronic specific heat is well described within the BCS theory with $\alpha = \Delta(0)/(k_B T_c) = 1.764$, where $2\Delta(0)$ is the full superconducting

gap, while for (4) the data indicate a slight enhancement of α up to 1.825 (see Supporting Information, Figures S3–S6). Main parameters, including critical temperature in the zero magnetic field (T_c) , normalized specific heat jump $(\Delta C_e/(\gamma_{\rm N}T_c))$, Debye temperature $(\Theta_{\rm D})$, Ginzburg–Landau parameter (κ) , and experimental $(\gamma_{\rm N})$ and calculated $(\gamma_{\rm bare})$ Sommerfeld coefficients, describing the superconducting state and electronic properties of the Mo₄Ga₂₁-based compounds are shown in Table 1.

The superconducting coherence length ξ can be estimated from the measured upper critical field $\mu_0H_{c2}(0)$ using the Ginzburg–Landau relation: $\mu_0H_{c2}(0)=\Phi_0/(2\pi\xi^2)$, where $\Phi_0=hc/(2e)$ is the flux quantum. The Ginzburg–Landau parameter $\kappa=\lambda/\xi$, where λ is the magnetic field penetration depth, was calculated as $\kappa=1/\sqrt{2\mu_0H_{c2}(0)/\mu_0H_c(0)}$. The Ginzburg–Landau parameter of $\kappa>1/\sqrt{2}$ clearly indicates the type-II superconductivity for (1)-(4). Accordingly, the upper critical field at zero temperature $\mu_0H_{c2}(0)$ is much larger than the lower critical field $\mu_0H_{c1}(0)$, and the thermodynamic critical field calculated as $\mu_0H_c(0)=1.382\alpha T_c\gamma^{1/2}$ within the α -model³² shows intermediate values (Table 1).

The parameters listed in Table 1 raise an interesting question: what trends can be proposed to explain the evolution of critical temperature in this series of isomorphous compounds. Taking into account the metallic behavior in the normal state and the good match of the electronic specific heat with the BCS predictions, the nature of the superconducting state in the family of Mo₄Ga₂₁-based superconductors should be closely connected with the electronic properties at the Fermi surface. Notably, the normal-state Sommerfeld coefficient, γ_N , is larger than the calculated one, γ_{bare} , because of the electron-phonon coupling. The electron-phonon coupling constant $\lambda_{\rm ep}$ can be calculated using the equation: $\gamma_{\rm N}/\gamma_{\rm bare}=1$ + λ_{ep} . Clearly, the λ_{ep} values indicate moderate or strong electron—phonon coupling in (1)—(4) (Table 1). The normalstate Sommerfeld coefficient is proportional to the electronic density of states at the Fermi energy. Accordingly, the critical temperature correlates well with γ_N for the title compounds, except Mo₄Ga₂₀Sb, for which the enhanced value of T_c is observed. This enhancement is in line with the increased value of α seen in the electronic specific heat and may be due to the increased role of the electron-phonon coupling. Strong electron-phonon coupling in the superconducting state was reported for Mo₄Ga_{21-x- δ}Sn_x²⁶ with $T_c = 5.85$ K, Mo₆Ga₃₁² (8.2 K)-, and Mo₈Ga₄₁²¹ (9.8 K)-related superconductors.

Figure 4 summarizes critical temperatures of the Mo-based endohedral cluster superconductors with the strong and weak coupling regimes shown in red and blue colors, respectively, according to the results obtained from the α -model. Clearly, the strongly coupled superconductors exhibit higher critical temperatures. Within the isoelectronic compounds (2) and (3), the critical temperature is suppressed by the chemical pressure because Se has a smaller covalent radius than Te. Thus, higher values of T_c can be expected for the superconductors containing elements with higher values of Z. Moreover, the critical temperature is governed by the valence electron count: it increases reaching the value of T_c = 9.8 K for Mo₈Ga₄₁, when the number of valence electrons decreases. Here, the Mo₄Ga₂₁-based solid solutions are useful in the study of relations between VEC and T_c . In the case of (1)-(3), limited solid solutions are formed because of the mixed occupancy of the (0; 0; 0) position by Ga and chalcogens (see Supporting Information, Table S1). These solid solutions

Table 1. Parameters of the Superconducting and Normal States of the Mo₄Ga₂₁-Based Compounds

	$Mo_4Ga_{20.38(1)}S_{0.62(1)}$	$\mathrm{Mo_4Ga_{20}Se}$	$\mathrm{Mo_4Ga_{20}Te}$	$Mo_4Ga_{20}Sb$
$T_{\rm c}$ [K]	5.1	3.3	4.6	6.6
$\mu_0 H_{c2}(0)$ [mT]	1100(30)	132(9)	251(7)	693(8)
$\mu_0 H_{c1}(0)$ [Oe]	48(2)	46(10)	74(4)	69(1)
$2\Delta(0)$ [meV], α	1.6, $\alpha = \alpha_{BCS}$	1.0, $\alpha = \alpha_{BCS}$	1.4, $\alpha = \alpha_{BCS}$	2.1, $\alpha = 1.825$
$\Delta C_{ m e}/(\gamma_{ m N}T_{ m c})$	1.43	1.43	1.43	1.53
$\Theta_{\mathrm{D}}\left[\mathrm{K} ight]$	294	281	278	287
$\mu_0 H_c(0)$ [Oe]	479	257	440	660
κ, ξ [nm], λ [nm]	16.3, 17, 277	3.6, 50, 180	4.0, 36, 144	7.4, 22, 163
$\gamma_{\mathrm{N}} \; [\mathrm{mJ} \; \mathrm{mol}^{-1} \; \mathrm{K}^{-2}]$	39.0	27.0	41.2	42.3
$\gamma_{\rm bare}~[{ m mJ~mol^{-1}~K^{-2}}]$	16.8	16.3	19.7	19.1
$\lambda_{ m ep}$	1.3	0.7	1.1	1.2

possess variable VEC in the range between 22.125 and 22.5 $\overline{\rm e}$ per Mo atom, for which a detailed trend of $T_{\rm c}$ can be established. Such trends can be further used for the deliberate synthesis of new endohedral cluster superconductors with the enhanced functional characteristics.

In conclusion, the family of Mo₄Ga₂₁-based superconductors now encompasses five representatives. Mo₄Ga_{20.38(1)}S_{0.62(1)}, Mo₄Ga₂₀Se, Mo₄Ga₂₀Te, and Mo₄Ga₂₀Sb prepared in this study crystallize in the common structure type, in which S, Se, Te, and Sb atoms center the cuboctahedral position. In the Mo₈Ga₄₁- and Mo₆Ga₃₁-related superconductors, this position is centered by the Ga atoms. On the one hand, the Mo-Ga framework demonstrates the special stability giving rise to at least seven superconducting compounds. On the other hand, it supports various chemical substitutions: the cuboctahedral position can be occupied by Ga atoms or by more electronegative elements, such as Sb or chalcogens. It is interesting to check if this position could be occupied by electropositive elements, such as alkaline-earth metals, capable of donating their valence electrons directly to the Mo-Ga framework and thus changing the critical temperature. Such substitutions can further extend the family of Mo₄Ga₂₁-based superconductors providing new intermetallic compounds with functional properties.

METHODS

Synthesis. $Mo_4Ga_{20.38(1)}S_{0.62(1)}$, $Mo_4Ga_{20}Se$, $Mo_4Ga_{20}Te$, and Mo₄Ga₂₀Sb compounds were synthesized using the standard ampule technique. Elemental Mo (powder, 4N), Ga (pieces, 5N), S (powder, 4N), Se (granules, 5N), Te (powder, 5N), and Sb (powder, 5N) were mixed according to the compositions of $Mo_4Ga_{21-x}E_x$ (E = S, Se, Te, Sb; x = 0.25, 0.5, 0.75, 1, and 1.25) and placed inside silica ampules, which were evacuated to a residual pressure of 5×10^{-3} mbar and flame sealed. For annealing, the programmable laboratory furnaces were used. In the case of E = Se, Te, and Sb, the samples were annealed at 600 °C for 7 days, cooled to room temperature in the shut-off furnace, finely ground, annealed at 600 °C for another 5 days, and quenched into cold water. In the case of E = S, the samples were annealed at 700 °C for 5 days, finely ground, annealed for another 5 days at 700 °C, and cooled to room temperature in the shut-off furnace. Single crystals of Mo₄Ga₂₀Te were synthesized using the joint flux of Ga and Te. The sample with the composition of MoGa_{47.5}Te_{2.5} and the total mass of 2 g was annealed at 1000 $^{\circ}\text{C}$ for 48 h and cooled to 400 °C at a rate of 5°/h. Excess of Ga metal was removed by centrifugation at room temperature, and the sample was subsequently treated with 2 M HCl for 24 h, washed with distilled water and acetone, and dried.

Characterization Techniques. Powder X-ray diffraction patterns were collected on a Malvern PANalytical X'Pert 3 Powder diffractometer equipped with a Cu X-ray source (CuK α radiation, λ

= 1.5418 Å) and Medipix PIXcel^{1D} detector. Rietveld refinements were performed in the Jana2006 program.³³ Data collection and refinement details are shown in Table S2 of Supporting Information. The refined parameters of atomic positions are presented in Tables S3-S6 for E = S, Se, Te, and Sb, respectively. Selected interatomic distances are given in Table S7. Single-crystal X-ray diffraction measurements were performed on a Bruker D8 Venture diffractometer equipped with a Mo X-ray source (Mo K α radiation, graphite monochromator, $\lambda = 0.71073$ Å) and Photon 100 CMOS detector. Absorption correction was performed numerically using indexed faces of the selected single crystal. Crystal structure refinements were performed within the full-matrix anisotropic approximation against | F^2 using the SHELXL-2018 program.³⁴ Details of data collection and refinement against the single-crystal X-ray diffraction data for Mo₄Ga₂₀Te are presented in Table S8 of Supporting Information. The refined parameters of atomic positions are listed in Tables S9 and

Electronic Structure Calculations. Structural parameters obtained from the Rietveld refinements against the powder X-ray diffraction data were used for calculations of electronic structures. In the case of E = S, the GaS site was populated solely by S atoms. Calculations were performed within the framework of density functional theory using the full-potential local-orbital minimum basis band-structure FPLO code $^{3.5}$ (version 14.00-47). In the scalar relativistic regime, local density approximation was used to treat the exchange and correlation energy. $^{3.6}$ Integrations were performed by the improved tetrahedron method $^{3.7}$ on a grid of $1.6 \times 1.6 \times 1.0 \times$

Physical Properties. Magnetization measurements were performed using a Magnetic Properties Measurement System (MPMS-XL5 SQUID, Quantum Design) on powder samples enclosed in a polyethylene film. The diamagnetic contribution from the sample holder was corrected by measuring the reference pelletized samples. Measurements were conducted in the zero-field cooling (zfc) and field cooling (fc) conditions at temperatures between 1.8 and 10 K in a magnetic field of 10 Oe. Additionally, magnetization was measured in the zfc conditions at different temperatures by sweeping the magnetic field from 0 to 5 T. The normal-state magnetic susceptibility was measured in the fc conditions at temperatures between 10 and 300 K in 0.5 and 2 T magnetic fields. Heat capacity measurements were performed using a relaxation-type calorimeter of the heat capacity option of a physical property measurement system (PPMS, Quantum Design) on pelletized samples. The long-pulse technique was employed,³⁸ according to which a heat pulses of 30% temperature rise and 3τ measurement time were used, where τ is the first-order relaxation time constant. Measurements were performed by raising the temperature from 1.8 to 30 K in 0 and 3 T magnetic fields. The dual-slope analysis of the heat capacity data was performed in the PPMS MultiVu program (Quantum Design). Electrical resistance was measured by the standard four-probe technique using the resistivity option of PPMS (Quantum Design). For measurements, rectangularshaped pellets with typical dimensions of $8 \times 3 \times 2 \text{ mm}^3$ were prepared by pressing the powder samples at room temperature at an

external pressure of 4 kbar. Electrical contacts were made by attaching 100 μ m Cu wires to the pellets using silver-containing epoxy resin. Measurements were performed at temperatures between 1.8 and 300 K in a zero magnetic field.

ASSOCIATED CONTENT

Solution Supporting Information

The Supporting Information is available free of charge at https://pubs.acs.org/doi/10.1021/acs.chemmater.0c02311.

Powder and single-crystal X-ray diffraction results, calculated electronic structures, and description of physical properties, including magnetic susceptibility, magnetization, electrical resistivity, and heat capacity, and CCDC 2004519-2004523 (PDF)

AUTHOR INFORMATION

Corresponding Author

Valeriy Yu. Verchenko — Department of Chemistry, Lomonosov Moscow State University, 119991 Moscow, Russia; National Institute of Chemical Physics and Biophysics, 12618 Tallinn, Estonia; orcid.org/0000-0002-8000-425X; Email: valeriy.verchenko@gmail.com

Authors

Alexander O. Zubtsovskii — Department of Chemistry, Lomonosov Moscow State University, 119991 Moscow, Russia; Experimental Physics VI, Center for Electronic Correlations and Magnetism, Institute of Physics, University of Augsburg, 86135 Augsburg, Germany

Danil S. Plenkin – Department of Chemistry, Lomonosov Moscow State University, 119991 Moscow, Russia

Alexey V. Bogach – Prokhorov General Physics Institute of the Russian Academy of Sciences, 119991 Moscow, Russia

Zheng Wei – Department of Chemistry, University at Albany, SUNY, Albany 12222, New York, United States

Alexander A. Tsirlin – Experimental Physics VI, Center for Electronic Correlations and Magnetism, Institute of Physics, University of Augsburg, 86135 Augsburg, Germany

Evgeny V. Dikarev — Department of Chemistry, University at Albany, SUNY, Albany 12222, New York, United States;
orcid.org/0000-0001-8979-7914

Andrei V. Shevelkov — Department of Chemistry, Lomonosov Moscow State University, 119991 Moscow, Russia; o orcid.org/0000-0002-8316-3280

Complete contact information is available at: https://pubs.acs.org/10.1021/acs.chemmater.0c02311

Notes

The authors declare no competing financial interest.

ACKNOWLEDGMENTS

The work is supported by the Russian Science Foundation, grant no. 17-13-01033. V.Y.V. is grateful for the financial support from the Mobilitas program of the European Science Foundation, grant no. MOBJD449. A.A.T. appreciates the financial support by the Federal Ministry for Education and Research under the Sofja Kovalevskaya Award of the Alexander von Humboldt Foundation. Z.W. and E.V.D. thank the National Science Foundation for supporting structural studies under grant no. CHE-1955585.

REFERENCES

- (1) Xu, H.; Holgate, T.; He, J.; Su, Z.; Tritt, T. M.; Kleinke, H. New Ternary Arsenides for High-Temperature Thermoelectric Applications. *J. Electron. Mater.* **2009**, *38*, 1030–1036.
- (2) Gascoin, F.; Rasmussen, J.; Snyder, G. J. High temperature thermoelectric properties of $Mo_3Sb_{7-x}Te_x$ for x = 1.6 and 1.5. *J. Alloys Compd.* **2007**, 427, 324–329.
- (3) Häussermann, U.; Boström, M.; Viklund, P.; Rapp, Ö.; Björnängen, T. FeGa₃ and RuGa₃: Semiconducting Intermetallic Compounds. *J. Solid State Chem.* **2002**, *165*, 94–99.
- (4) Amagai, Y.; Yamamoto, A.; Iida, T.; Takanashi, Y. Thermoelectric properties of semiconductorlike intermetallic compounds TMGa₃ (TM = Fe, Ru, and Os). *J. Appl. Phys.* **2004**, *96*, 5644.
- (5) Bogdanov, D.; Winzer, K.; Nekrasov, I. A.; Pruschke, T. Electronic properties of the semiconductor RuIn₃. *J. Phys.: Condens. Matter* **2007**. *19*, 232202.
- (6) Kasinathan, D.; Wagner, M.; Koepernik, K.; Cardoso-Gil, R.; Grin, Y.; Rosner, H. Electronic and thermoelectric properties of $RuIn_{3-x}A_x$ (A = Sn, Zn). *Phys. Rev. B: Condens. Matter Mater. Phys.* **2012**, 85, 035207.
- (7) Fredrickson, D. C.; Lee, S.; Hoffmann, R. The Nowotny Chimney Ladder Phases: Whence the 14 Electron Rule? *Inorg. Chem.* **2004**, *43*, 6159–6167.
- (8) Liu, W.-D.; Chen, Z.-G.; Zou, J. Eco-Friendly Higher Manganese Silicide Thermoelectric Materials: Progress and Future Challenges. *Adv. Energy Mater.* **2018**, *8*, 1800056.
- (9) Wollmann, L.; Nayak, A. K.; Parkin, S. S. P.; Felser, C. Heusler 4.0: Tunable Materials. *Annu. Rev. Mater. Res.* 2017, 47, 247–270.
- (10) Zhu, H.; He, R.; Mao, J.; Zhu, Q.; Li, C.; Sun, J.; Ren, W.; Wang, Y.; Liu, Z.; Tang, Z.; Sotnikov, A.; Wang, Z.; Broido, D.; Singh, D. J.; Chen, G.; Nielsch, K.; Ren, Z. Discovery of ZrCoBi based half Heuslers with high thermoelectric conversion efficiency. *Nat. Commun.* 2018, 9, 2497.
- (11) Liu, Y.; Sahoo, P.; Makongo, J. P. A.; Zhou, X.; Kim, S.-J.; Chi, H.; Uher, C.; Pan, X.; Poudeu, P. F. P. Large enhancements of thermopower and carrier mobility in quantum dot engineered bulk semiconductors. *J. Am. Chem. Soc.* **2013**, *135*, 7486–7495.
- (12) Canfield, P. C.; Thompson, J. D.; Beyermann, W. P.; Lacerda, A.; Hundley, M. F.; Peterson, E.; Fisk, Z.; Ott, H. R. Magnetism and heavy fermion-like behavior in the RBiPt series. *J. Appl. Phys.* **1991**, 70, 5800.
- (13) Fisk, Z.; Canfield, P. C.; Beyermann, W. P.; Thompson, J. D.; Hundley, M. F.; Ott, H. R.; Felder, E.; Maple, M. B.; Lopez de la Torre, M. A.; Visani, P.; Seaman, C. L. Massive electron state in YbBiPt. *Phys. Rev. Lett.* **1991**, *67*, 3310.
- (14) Goll, G.; Marz, M.; Hamann, A.; Tomanic, T.; Grube, K.; Yoshino, T.; Takabatake, T. Thermodynamic and transport properties of the non-centrosymmetric superconductor LaBiPt. *Phys. B* **2008**, 403, 1065–1067.
- (15) Butch, N. P.; Syers, P.; Kirshenbaum, K.; Hope, A. P.; Paglione, J. Superconductivity in the topological semimetal YPtBi. *Phys. Rev. B: Condens. Matter Mater. Phys.* **2011**, *84*, 220504.
- (16) Bende, D.; Wagner, F. R.; Grin, Y. 8-N Rule and Chemical Bonding in Main-Group MgAgAs-Type Compounds. *Inorg. Chem.* **2015**, *54*, 3970–3978.
- (17) Yannello, V. J.; Kilduff, B. J.; Fredrickson, D. C. Isolobal Analogies in Intermetallics: The Reversed Approximation MO Approach and Applications to CrGa₄- and Ir₃Ge₇-Type Phases. *Inorg. Chem.* **2014**, *53*, 2730–2741.
- (18) Yannello, V. J.; Fredrickson, D. C. Orbital Origins of Helices and Magic Electron Counts in the Nowotny Chimney Ladders: the 18-n Rule and a Path to Incommensurability. *Inorg. Chem.* **2014**, *53*, 10627–10631.
- (19) Yannello, V. J.; Fredrickson, D. C. Generality of the 18-n Rule: Intermetallic Structural Chemistry Explained through Isolobal Analogies to Transition Metal Complexes. *Inorg. Chem.* **2015**, *54*, 11385–11398.

- (20) Bezinge, A.; Yvon, K.; Decroux, M.; Muller, J. On the existence of binary Mo_8Ga_{41} and its properties. *J. Less-Common Met.* **1984**, 99, L27–L31.
- (21) Verchenko, V. Y.; Tsirlin, A. A.; Zubtsovskiy, A. O.; Shevelkov, A. V. Strong electron-phonon coupling in the intermetallic superconductor Mo₈Ga₄₁. *Phys. Rev. B* **2016**, *93*, 064501.
- (22) Fischer, O. Properties of high field superconductors, containing localized magnetic moments. *Helv. Phys. Acta* **1972**, *45*, 331.
- (23) Verchenko, V. Yu.; Zubtsovskii, A. O.; Tsirlin, A. A.; Wei, Z.; Roslova, M.; Dikarev, E. V.; Shevelkov, A. V. Mo6Ga31 endohedral cluster superconductor. **2020**, arXiv:2004.05425.
- (24) Xie, W.; Luo, H.; Phelan, B. F.; Klimczuk, T.; Cevallos, F. A.; Cava, R. J. Endohedral gallide cluster superconductors and superconductivity in ReGa₅. *Proc. Natl. Acad. Sci. U.S.A.* **2015**, *112*, E7048–E7054.
- (25) Shibayama, T.; Nohara, M.; Aruga Katori, H.; Okamoto, Y.; Hiroi, Z.; Takagi, H. Superconductivity in Rh₂Ga₉ and Ir₂Ga₉ without inversion symmetry. *J. Phys. Soc. Jpn.* **2007**, *76*, 073708.
- (26) Verchenko, V. Y.; Zubtsovskii, A. O.; Wei, Z.; Tsirlin, A. A.; Marcin, M.; Sobolev, A. V.; Presniakov, I. A.; Dikarev, E. V.; Shevelkov, A. V. Endohedral Cluster Superconductors in the Mo-Ga-Sn System Explored by the Joint Flux Technique. *Inorg. Chem.* **2019**, 58, 15552–15561.
- (27) Wolcyrz, M.; Andruszkiewicz, R.; Lukaszewicz, K. Structure of Mo₈Ga₄₁S. *Acta Crystallogr., Sect. C: Cryst. Struct. Commun.* **1989**, 45, 991–993
- (28) Verchenko, V. Y.; Mironov, A. V.; Wei, Z.; Tsirlin, A. A.; Dikarev, E. V.; Shevelkov, A. V. Crystal Growth of Intermetallics from the Joint Flux: Exploratory Synthesis through the Control of Valence Electron Count. *Inorg. Chem.* **2019**, *58*, 1561–1570.
- (29) Biltz, W. Raumchemie der festen Stoffe; Verlag von Leopold Voss: Leipzig, 1934.
- (30) Dronskowski, R. Computational Chemistry of Solid State Materials; WILEY-VCH Verlag GmbH & Co.: Weinheim, 2005.
- (31) Padamsee, H.; Neighbor, J. E.; Shiffman, C. A. Quasiparticle phenomenology for thermodynamics of strong-coupling superconductors. *J. Low Temp. Phys.* 1973, 12, 387–411.
- (32) Johnston, D. C. Elaboration of the α -model derived from the] theory of superconductivity. *Supercond. Sci. Technol.* **2013**, 26, 115011.
- (33) Petříček, V.; Dušek, M.; Palatinus, L. Crystallographic computing system JANA2006: General features. *Z. Kristallogr.* **2014**, 229, 345–352.
- (34) Sheldrick, G. M. Crystal structure refinement with SHELXL. Acta Crystallogr., Sect. C: Struct. Chem. 2015, 71, 3-8.
- (35) Koepernik, K.; Eschrig, H. Full-Potential Nonorthogonal Local-Orbital Minimum-Basis Band-Structure Scheme. *Phys. Rev. B: Condens. Matter Mater. Phys.* **1999**, 59, 1743.
- (36) Perdew, J. P.; Wang, Y. Accurate and Simple Analytic Representation of the Electron-Gas Correlation Energy. *Phys. Rev. B: Condens. Matter Mater. Phys.* **1992**, *45*, 13244.
- (37) Blöchl, P. E.; Jepsen, O.; Andersen, O. K. Improved Tetrahedron Method for Brillouin-Zone Integrations. *Phys. Rev. B: Condens. Matter Mater. Phys.* **1994**, 49, 16223.
- (38) Scheie, A. LongHCPulse: Long-Pulse Heat Capacity on a Quantum Design PPMS. J. Low Temp. Phys. **2018**, 193, 60-73.